Effect of lattice constant on pseudo Jahn-Teller polar distortion: Application to search for new multiferroic compounds

Guang Song and Weiyi Zhang*

National Laboratory of Solid State Microstructures and Department of Physics, Nanjing University, Nanjing 210093, China
and Collaborative Innovation Center of Advanced Microstructures, Nanjing University, Nanjing 210093, China

(Received 2 December 2015; revised manuscript received 23 June 2016; published 8 August 2016)

By analog to Maxwell construction for the first-order phase transition, the pseudo Jahn-Teller polar distortion arises naturally once the local bond length of transition-metal oxygen octahedra is enhanced beyond the inflexion point of pair potential into the concave-down dominated region. This concept is applied to search for the new multiferroic compounds for which we specifically choose the $(BaMnO_3)_1/(BaFeO_3)_1$ superlattice as a candidate. The large Ba radius favors the polar distortion in a $BaMnO_3$ layer, while the orbital-ordering-induced superexchange ferromagnetic coupling among Fe-Fe and double-exchange mediated ferromagnetic coupling among Fe-Mn ions stabilize the overall ferromagnetic insulator. A large magnetic moment of $7\mu_B$ per unit cell and electric polarization of 14.4 $\mu C\,cm^{-2}$ are obtained. Our study offers an important insight for designing robust multiferroic compounds in the future.

DOI: 10.1103/PhysRevB.94.064409

I. INTRODUCTION

The excellent multiferroic compounds must be insulating materials with large electric polarization and magnetization. Such materials have important application in information storage and spintronic devices because their magnetoelectric coupling property makes it possible to cross-control polarization or magnetization by a magnetic or electric field [1–3]. However, the multiferroic compounds are rare in nature due to the conflict requirements by electric polarization and magnetization. The empirical rules stipulate the so-called Matthias's "d^0-ness" of transition-metal ions for the spontaneous electric polarization [4] and the partially filled d shell for magnetization [5,6]. Furthermore, ferromagnetic states are usually associated with metals [7], and a complex d-orbital-ordering configuration is required to produce insulating ferromagnetic states [8,9].

Therefore, improving multiferroic property requires one to reconcile the contradictory restrictions imposed by ferroelectricity and ferromagnetism [10–12]. If both required conditions are to be fulfilled satisfactorily, two types of transition-metal ions are needed for two different functionalities, but the strong magnetoelectric coupling cannot be ensured since the ferroelectricity and ferromagnetism can be independent of each other [13,14]. Although more complex, noncollinear, magnetic (electric polarization) structures might solve the coupling problem, it is always associated with one strong magnetization (polarization) component and one induced weak polarization (magnetization) component [15–18].

To overcome the deadlock of the above empirical rules, efforts have been made to circumvent Matthias's d^0-ness rule in practice [4]. As is well known, perovskite $BaTiO_3$ is a prototypical ferroelectric compound with Ti^{4+} ions fulfilling the d^0-ness requirements [6], but the structurally similar $CaTiO_3$ and $SrTiO_3$ compounds are not ferroelectric [19,20]. This shows that d^0-ness is obviously not a sufficient condition for ferroelectricity. By comparing the ionic radii of alkali-earth elements Ca (0.99 Å), Sr (1.13 Å), and Ba (1.35 Å), the large average Ti-O bond length stabilizes the polar distortion in the ferroelectric state. Such tendency is not only valid for $RTiO_3$ (R = Ca, Sr, Ba) compounds, but also holds true for partially filled d-shell perovskites. In the recent studies on epitaxially strained $SrMnO_3$ heterostructure [21–24] and Ba-doped $SrMnO_3$ bulk samples [25–27], ferroelectric polarizations are observed either under large epitaxial strain ($e > 1.0\%$ or $e < -1.2\%$) [21] or when Ba doping is larger than 45% [25]. These observations suggested that d^0-ness is not even a necessary condition for ferroelectric instability.

Among others, the non-d^0-ness perovskite multiferroics are predicted by Bhattacharjee *et al.* [28] and Rondinelli *et al.* [29] based on the soft-phonon modes of $CaMnO_3$ and $BaMnO_3$. These theoretical studies found that the polar distortion mode and antiferrodistortive mode usually compete with each other in manganese-based perovskite; the polar distortion mode survives only when the antiferrodistortive mode is suppressed by large A-site atoms such as Ba. The similar multiferroic is also predicted in TTF-CA organic molecular crystals where polar distortion is induced by Peierls' instability [30]. These multiferroics involve antiferromagnetic structure, and the cross tuning of order parameters is difficult. For the mixed-valence perovskites such as $(La,Pr)_{1-x}Ca_xMnO_3$ [31] and $La_{1/2}Ca_{1/2}MnO_3$ [32], site-centered charge ordering (SC-CO) and double-exchange-mediated bond-centered charge ordering (BC-CO) exist simultaneously. The charge ordering and noncollinear spin configuration of Zener polarons break the space-inversion symmetry and offer a new mechanism for multiferroics. It is noted that careful tuning of bond lengths and bond angles of MnO_6 octahedra is an important step to achieve multiferroism.

The mechanism of ferroelectricity is an old and interesting topic and have been studied by many groups. The first microscopic model for the $BaTiO_3$ ferroelectric was proposed by Slater in 1950 [33]. In his model, the dipolar moment was induced by the off-centering of Ti^{4+} ions of TiO_6 octahedra and the cooperative alignment of dipoles was stabilized by long-range dipolar interaction. To treat all atoms on equal footing, Cochran [34] was able to significantly lower the polar

*Corresponding author: wyzhang@nju.edu.cn

distortion energy using the lattice dynamics. The off-center displacement eigenvectors along ⟨111⟩, ⟨110⟩, and ⟨001⟩ were predicted from the soft-phonon modes of a dynamical matrix. Cochran's phenomenological model suggested that short-range interaction favors a high-symmetrical phase, while long-range interaction favors polar distortion. However, these are classical models and do not take the quantum effect into consideration. As shown by Bersuker in 1966 [35], the electronic covalence bonding between Ti and O plays a very important role in addition to long-range dipolar interaction. By calculating the second-order Jahn-Teller effect (also called pseudo Jahn-Teller effect), Bersuker obtained the complete energy landscape of local vibronic energy. The eight degenerate polar distortion modes with minimum energy were found along the ⟨111⟩ directions of TiO_6 octahedra if covalence bonding is included. This is further confirmed by the first-principles calculation [36]. Using the order-disorder transition model [37], excellent agreements are obtained with both the x-ray diffraction experiment [37] and the ferroelectric transition temperatures of three crystal phases of $BaTiO_3$ [38].

With the miniaturization of electronic devices, there exist strong demands for ferroelectric thin films. So a crucial issue concerning ferroelectricity is to discern whether the polar distortion is a global phenomenon relating to the long-range dipolar interaction or a local phenomenon relating to the pseudo Jahn-Teller effect. A recent experiment [39] showed that $SrTiO_3$ thin films are relaxor ferroelectrics, Sr-vacancy-induced nanopolar regions preexist in samples, and external strain establishes the correlation among nanopolar regions. To quantitatively address this issue, two theoretical works by Garćia-Lastra [40] and Aramburu [41] have extensively analyzed the contributions from the local pseudo Jahn-Teller effect and the long-range dipolar interaction. They show that the off-centering of an impurity is determined more by the local pseudo Jahn-Teller effect than the long-range dipolar interaction. Consistent with the other models mentioned above, they also found that an enlarging lattice constant always favors the polar distortion, while a reducing lattice constant does the opposite. This general trend can be understood from the schematic pair potential drawn in Fig. 1, where the pair potential is concave-down and has slow positive slope at long bond length, while it is concave-up and has sharp negative slope at short bond length. When bond length b deviates slightly from the equilibrium bond length b_0, there is always a recovery force which brings the crystal back to equilibrium. However, the uniform bond-length configuration can become unstable when the deviation goes beyond b_i, the so-called inflexion point, where the second derivative is zero. When that happens, crystal enters into a dimerized structure. The long (b_l) and short (b_s) bond lengths are obtained by searching for the minima of potential landscape at a fixed average bond length b, a process similar to Maxwell construction of the first-order phase transition.

The schematic diagram suggests that a ferroelectric instability can be induced by enlarging the lattice constant so that the local bond length is large enough to stay in the concave-down region of pair potential. This is exactly what has happened for the ferroelectric property in $BaTiO_3$ or Ba-doped $SrMnO_3$ compounds [6,25–27]. For compounds involving different bonding types, the inflexion point may vary, but the conclusion that a large lattice constant favors polar distortion remains valid.

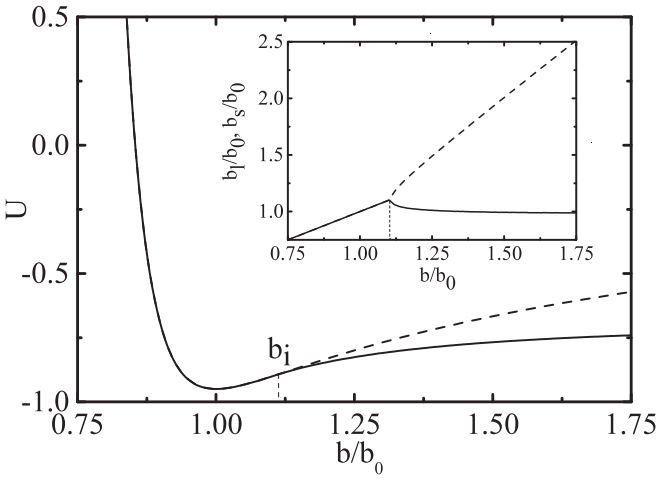

FIG. 1. The schematic diagram of pair potential of transition-metal oxygen octahedron. The energies of polar and nonpolar structures are illustrated by solid and dashed lines which deviate from each other at the inflexion point. The inset illustrates the long (b_l) and short (b_s) bond lengths as functions of averaged bond length $b = 0.5(b_l + b_s)$.

II. DESIGN MULTIFERROIC WITH SUPERLATTICES

The fact that the large pseudo Jahn-Teller effect, rather than the d^0-ness of transition-metal ions, is the precursor for ferroelectric instability considerably softens the previous conflict requirements on d-shell electrons regarding the ferroelectric and ferromagnetic properties. This, in turn, assures strong magnetoelectric coupling which makes the cross-control of electric and magnetic properties possible. Thus, to design a perovskite-type multiferroic insulator at atomic scale with strong electric polarization and magnetization, one has to address the following issues: (1) transition-metal ions centered oxygen octahedra is pseudo Jahn-Teller effect active; (2) ionic radii of alkali-earth elements are large so that the local equilibrium bond length and inflexion point are as close as possible; (3) the nearest-neighbor transition-metal ions are arranged in such a way so that their d-orbital configurations maximize the double-exchange or superexchange ferromagnetic couplings [42,43] and realize the insulator state as required by an excellent multiferroic compound.

As a proof of concept, we propose a binary superlattice $(BaMnO_3)_1/(BaFeO_3)_1$ (BMO/BFO) as a possible candidate for a ferroelectric ferromagnetic multiferroic. The physical reasoning behind this choice is as follows: As shown by Ba-doped $SrMnO_3$, the Mn centered oxygen octahedra undergo a ferroelectric transition as Mn-O bond lengths cross the inflexion point. However, theoretical study showed that the bulk $BaMnO_3$ is a G-type antiferromagnetic (G-AFM) multiferroic [29] due to the weak superexchange interaction among neighboring Mn-$d_{t_{2g}}$ electrons, which runs counter to the required ferromagnetism. In order to microstructurally manipulate the double-exchange and superexchange interactions to realize the global ferromagnetic ordering, we specifically

select the ferromagnetic insulator $BaFeO_3$ as a complementary component [44]. Unlike Mn^{4+} ions with all electrons in their $d_{t_{2g}}$ orbitals, Fe^{4+} ions have one electron in their d_{e_g} orbitals if they are in the high-spin states. Since Fe^{4+} ions are well-known Jahn-Teller active ions, crystal-symmetry reduction is a necessary outcome to lower the electronic energy. The resulting structure stabilizes "antiferro-" orbitally ordered structure with alternating $d_{3x^2-r^2}$- and $d_{3y^2-r^2}$-orbital ordering among neighboring Fe ions [45]. This orbital ordering activates the superexchange ferromagnetic coupling, similar to that which occurred in the undoped $LaMnO_3$ compound [46], which supports the intraplane ferromagnetism. For the binary superlattices BMO/BFO, Mn^{4+} ions and Fe^{4+} ions are mutually nearest neighbors along the c axis. The missing Mn-d_{e_g} electrons of Mn-O-Fe chains make it resemble a mixed-valence system, and thus the double-exchange ferromagnetic interaction functions. Since the electron hopping parameters via d_{e_g} orbitals are much larger than those via $d_{t_{2g}}$ orbitals, it is hoped that these superexchange and double-exchange ferromagnetic interactions among Fe-Fe and Fe-Mn will overwhelm the antiferromagnetic superexchange interaction among Mn-Mn ions.

In this paper, the first-principles calculations on BMO/BFO superlattices were performed using a plane-wave basis set with cutoff energy of 600 eV and the projector augmented-wave method (PAW) [47] as implemented in the Vienna *ab initio* simulation package (VASP) code [48,49]. We used the generalized gradient approximation (GGA) with the Perdew-Burke-Erzenhof (PBE) parametrization to describe the electronic exchange and correlation effects [50]. Each self-consistent electronic calculation is converged to 10^{-6} eV and the tolerance force is set to 0.005 eV/Å for the ionic relaxation. In $BaMnO_3/BaFeO_3$ superlattices, we used a $\sqrt{2}\times\sqrt{2}\times 1$ (20 atoms) unit cell with a $5\times5\times5$ Γ-centered k-point sampling. The projector augmented-wave potentials explicitly include 10 valence electrons for Ba ($5s^25p^66s^2$), 14 for Fe ($3p^63d^64s^2$), 13 for Mn ($3p^63d^54s^2$), and 6 for O ($2s^22p^4$). To address the issue of the strong correlations on Fe-d and Mn-d orbitals, both the rotationally invariant Liechtenstein approach to GGA+U [51] and Heyd, Scuseria, and Ernzerhof (HSE) screened hybrid functionals methods [52,53] were adopted. To study the competition among various different magnetically ordered states, we have considered the ferromagnetically (FM) ordered state, the chain-type antiferromagnetically (C-AFM) ordered state, the nearest-neighbor antiferromagnetically (G-AFM) ordered state, and the interplane antiferromagnetically (A-AFM) ordered state.

III. RESULTS AND DISCUSSIONS

To derive the possible ground-state structure considered in our paper, we adopt the same method as used by Bousquet *et al.* [54]. We start from the high-symmetry $P4/mmm$ phase of $BaMnO_3/BaFeO_3$ superlattices with 20 atoms in a unit cell and relax the crystal symmetry as dictated by the frozen phonon method (see Table I in Supplemental Material [55]). In this way, the $Pmc2_1$ crystal structure yields the lowest energy (see Table II in Supplemental Material [55]). The total-energy, band-gap, and electron occupation numbers of four magnetically ordered states are calculated using the hybrid functionals method. As shown in Table I, the combination of Mn^{4+} and Fe^{4+} in a superlattice structure does enhance the double-exchange and superexchange ferromagnetic couplings and makes a ferromagnetic ground state.

TABLE I. The energy (E), band gap (E_g), and electric polarization (P) of a $Pmc2_1$ structure for four magnetically ordered states. Also listed are the electron occupation numbers and magnetic moments for Fe and Mn ions. All quantities are calculated using the HSE06 method except P calculated using GGA+U, with $U = 3.5$ eV and $J = 0.8$ eV to save CPU time. The energy of the FM state is set as a reference state.

	FM	C-AFM	G-AFM	A-AFM
E (eV)	0.000	0.027	0.138	0.018
E_g (eV)	0.728	1.268	1.560	1.432
n_d^{Fe}	5.63	5.65	5.66	5.63
n_d^{Mn}	4.90	4.90	4.89	4.89
μ_d^{Fe} (μ_B)	3.46	3.46	3.39	3.40
μ_d^{Mn} (μ_B)	2.92	2.86	2.82	2.89
P (μC cm^{-2})	14.4	22.4	20.1	13.0

The Jahn-Teller distortion and polar distortion are clearly demonstrated in the fully relaxed $Pmc2_1$ structure shown in Fig. 2. The Jahn-Teller effect of Fe^{4+} ($t_{2g}^3e_g^1$) ions distorts the FeO_6 octahedra in such a way so that intraplane $3x^2-r^2/3y^2-r^2$ orbital ordering doubles the primary cell and makes the superlattices an insulator. In addition, both MnO_6 and FeO_6 octahedra manifest polar distortion, though the major ferroelectricity comes from MnO_6 octahedra. This property is also consistent with that of the Ba-doped $SrMnO_3$ compound. Using the Berry phase method [56], the electric polarization of the $Pmc2_1$ phase is calculated with respect to the nonpolar reference $P4/mbm$ structure, and a robust value of 14.4 μC cm^{-2} along the intraplane [110] axis is obtained for the FM ordered state (see Fig. 2(c) in the Supplemental

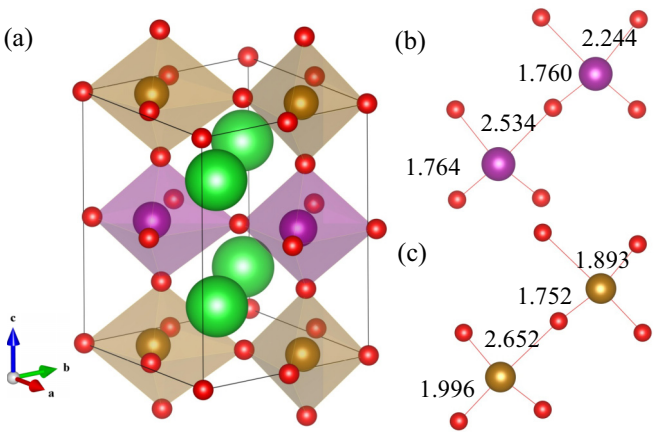

FIG. 2. The relaxed $Pmc2_1$ structure of the BMO/BFO superlattice within the HSE06 method. (a) The overall crystal structure of the BMO/BFO superlattice. The top and bottom layers denote the FeO_6 octahedra and the middle layer denotes the MnO_6 octahedra; (b) the intraplane bond lengths of MnO_6 octahedra; (c) the intraplane bond lengths of FeO_6 octahedra. The red, golden, magenta, and green spheres refer to O, Fe, Mn, and Ba atoms, respectively.

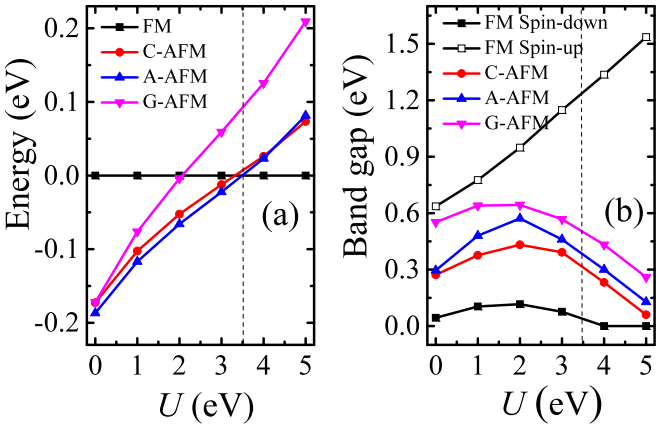

FIG. 3. The energies and band gaps of the $Pmc2_1$ structure calculated within the GGA+U method for four magnetically ordered states. (a) Energy; (b) band gap. The black line with the solid square refers to the band gap of spin-up bands, while the hollow square refers to the band gap of spin-down bands.

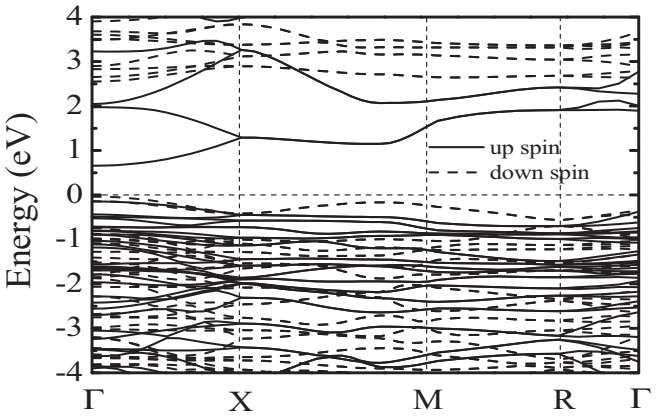

FIG. 4. The spin-resolved electronic band structure of the FM $Pmc2_1$ phase calculated using the HSE06 method.

Material [55]). The polar distortion of MnO_6 octahedra originates from the same mechanism as $BaMnO_3$ [28,29], while site-centered and bond-centered charge orderings are also involved in the making of the ferroelectricity of BMO/BFO superlattices [31,32].

The relative stabilities of the four magnetic states of the $Pmc2_1$ structure of the $(BaMnO_3)_1/(BaFeO_3)_1$ superlattice have also been analyzed within the GGA+U method. The energies and band gaps are shown in Fig. 3 as functions of Coulomb U. The Hund coupling parameter J is fixed at 0.8 eV for easy comparison. As shown in Fig. 3(a), the FM ordered state strongly competes with the A-AFM ordered state. The FM ordered state becomes the ground state when Coulomb repulsion $U > 3.5$ eV; this range of U is common for Fe and Mn d electrons. The band gap of the FM ordered state in Fig. 3(b) shows nonmonotonic behavior as U increases; the FM ordered state can be either an insulator or a spin fully polarized half metal. The HSE06 hybrid density functional method consistently predicts the FM ordered state as a possible ground state with a sizable band gap. This suggests that better treatment of electronic correlation in the BMO/BFO superlattice is very important.

To show an overall view of the ferroelectric ferromagnetic insulator of the $Pmc2_1$ phase, the spin-resolved band structures are presented in Fig. 4. The band structures belong to a direct band-gap insulator with the band gaps located at the Γ point for both spin-up and spin-down bands. The band gap for spin-up bands is much smaller than that for spin-down bands, and thus determines the overall band gap. The overall band gap of 0.728 eV is relatively large among the available ferroelectric ferromagnetic insulators [24]. It is well known that a large band gap facilitates the electric cross control of magnetic orderings. Unlike the multiferroic thin films prepared on compressive or tensile strained substrates where polarization and magnetization reversals are opposed by substrate imposed strain, the electric polarization or magnetization of BMO/BFO superlattices can be easily swept by an external field just like any ordinary ferroelectric or ferromagnetic compounds.

IV. CONCLUSION

In summary, we have shown in this paper that the ferroelectric instability is associated with the concave-down feature of pair potential. The strong pseudo Jahn-Teller effect, rather than the d^0-ness property of transition-metal ions, is the prerequisite for ferroelectricity. This criterion offers an opportunity to design the multiferroic materials by choosing the right transition-metal elements and right crystal structures to enhance the double-exchange and superexchange ferromagnetic couplings. As an example, the BMO/BFO superlattice was chosen to demonstrate the design tactic for the robust ferroelectric ferromagnetic multiferroic insulator.

ACKNOWLEDGMENTS

This work was supported in part by the National Natural Science Foundation of China under Grant No. 11474148. Financial support from the Outstanding Ph.D. Program B of Nanjing University is also gratefully acknowledged. Part of the numerical calculations were carried out in the High Performance Computing Center (HPCC) of Nanjing University. We thank Sujie Zhang for reviewing the manuscript.

[1] S. W. Cheong and M. Mostovoy, Nat. Mater. **6**, 13 (2007).
[2] W. Eerenstein, N. D. Mathur, and J. F. Scott, Nature (London) **442**, 759 (2006).
[3] R. Ramesh and N. A. Spaldin, Nat. Mater. **6**, 21 (2007).
[4] B. T. Matthias, Phys. Rev. **75**, 1771 (1949).
[5] N. A. Hill, J. Phys. Chem. B **104**, 6694 (2000).
[6] R. E. Cohen, Nature (London) **358**, 136 (1992).
[7] D. I. Khomskii and G. A. Sawatzky, Solid State Commun. **102**, 87 (1997).
[8] K. Gupta, P. Mahadevan, P. Mavropoulos, and M. Ležaić, Phys. Rev. Lett. **111**, 077601 (2013).
[9] G. Song and W. Y. Zhang, Sci. Rep. **4**, 4564 (2014).

[10] D. I. Khomskii, J. Magn. Magn. Mater. **306**, 1 (2006).
[11] C. A. F. Vaz, J. Hoffman, C. H. Ahn, and R. Ramesh, Adv. Mater. **22**, 2900 (2010).
[12] M. J. Pitcher, P. Mandal, M. S. Dyer, J. Alaria, P. Borisov, H. Niu, J. B. Claridge, and M. J. Rosseinsky, Science **347**, 420 (2015).
[13] J. Wang, J. B. Neaton, H. Zheng, V. Nagarajan, S. B. Ogale, B. Liu, D. Viehland, V. Vaithyanathan, D. G. Schlom, U. V. Waghmare, N. A. Spaldin, K. M. Rabe, M. Wuttig, and R. Ramesh, Science **299**, 1719 (2003).
[14] T. Kimura, T. Goto, H. Shintani, K. Ishizaka, T. Arima, and Y. Tokura, Nature (London) **426**, 55 (2003).
[15] Y. Kitagawa, Y. Hiraoka, T. Honda, T. Ishikura, H. Nakamura, and T. Kimura, Nat. Mater. **9**, 797 (2010).
[16] W. Wang, J. Zhao, W. Wang, Z. Gai, N. Balke, M. Chi, H. N. Lee, W. Tian, L. Zhu, X. Cheng, D. J. Keavney, J. Yi, T. Z. Ward, P. C. Snijders, H. M. Christen, W. Wu, J. Shen, and X. Xu, Phys. Rev. Lett. **110**, 237601 (2013).
[17] Y. W. Windsor, S. W. Huang, Y. Hu, L. Rettig, A. Alberca, K. Shimamoto, V. Scagnoli, T. Lippert, C. W. Schneider, and U. Staub, Phys. Rev. Lett. **113**, 167202 (2014).
[18] S. M. Disseler, J. A. Borchers, C. M. Brooks, J. A. Mundy, J. A. Moyer, D. A. Hillsberry, E. L. Thies, D. A. Tenne, J. Heron, M. E. Holtz, J. D. Clarkson, G. M. Stiehl, P. Schiffer, D. A. Muller, D. G. Schlom, and W. D. Ratcliff, Phys. Rev. Lett. **114**, 217602 (2015).
[19] J. H. Haeni, P. Irvin, W. Chang, R. Uecker, P. Reiche, Y. L. Li, S. Choudhury, W. Tian, M. E. Hawley, B. Craigo, A. K. Tagantsev, X. Q. Pan, S. K. Streiffer, L. Q. Chen, S. W. Kirchoefer, J. Levy, and D. G. Schlom, Nature (London) **430**, 758 (2004).
[20] O. Diéguez, K. M. Rabe, and D. Vanderbilt, Phys. Rev. B **72**, 144101 (2005).
[21] J. H. Lee and K. M. Rabe, Phys. Rev. Lett. **104**, 207204 (2010).
[22] G. Song and W. Y. Zhang, J. Phys. Soc. Jpn. **84**, 044713 (2015).
[23] C. Becher, L. Maurel, U. Aschauer, M. Lilienblum, C. Magén, D. Meier, E. Langenberg, M. Trassin, J. Blasco, I. P. Krug, P. A. Algarabel, N. A. Spaldin, J. A. Pardo, and M. Fiebig, Nat. Nanotechnol. **10**, 661 (2015).
[24] L. Maurel, N. Marcano, T. Prokscha, E. Langenberg, J. Blasco, R. Guzmán, A. Suter, C. Magén, L. Morellón, M. R. Ibarra, J. A. Pardo, and P. A. Algarabel, Phys. Rev. B **92**, 024419 (2015).
[25] H. Sakai, J. Fujioka, T. Fukuda, D. Okuyama, D. Hashizume, F. Kagawa, H. Nakao, Y. Murakami, T. Arima, A. Q. R. Baron, Y. Taguchi, and Y. Tokura, Phys. Rev. Lett. **107**, 137601 (2011).
[26] G. Giovannetti, S. Kumar, C. Ortix, M. Capone, and J. van den Brink, Phys. Rev. Lett. **109**, 107601 (2012).
[27] R. Nourafkan, G. Kotliar, and A. M. S. Tremblay, Phys. Rev. B **90**, 220405 (2014).
[28] S. Bhattacharjee, E. Bousquet, and P. Ghosez, Phys. Rev. Lett. **102**, 117602 (2009).
[29] J. M. Rondinelli, A. S. Eidelson, and N. A. Spaldin, Phys. Rev. B **79**, 205119 (2009).
[30] G. Giovannetti, S. Kumar, A. Stroppa, J. van den Brink, and S. Picozzi, Phys. Rev. Lett. **103**, 266401 (2009).
[31] D. V. Efremov, J. van den Brink, and D. I. Khomskii, Nat. Mater. **3**, 853 (2004).
[32] G. Giovannetti, S. Kumar, J. van den Brink, and S. Picozzi, Phys. Rev. Lett. **103**, 037601 (2009).
[33] J. C. Slater, Phys. Rev. **78**, 748 (1950).
[34] W. Cochran, Adv. Phys. **9**, 387 (1960).
[35] I. B. Bersuker, Phys. Lett. **20**, 589 (1966).
[36] R. E. Cohen and H. Krakauer, Phys. Rev. B **42**, 6416 (1990).
[37] R. Comes, M. Lambert, and A. Guinier, Solid State Commun. **6**, 715 (1968).
[38] W. Zhong, D. Vanderbilt, and K. M. Rabe, Phys. Rev. Lett. **73**, 1861 (1994).
[39] H. W. Jang, A. Kumar, S. Denev, M. D. Biegalski, P. Maksymovych, C. W. Bark, C. T. Nelson, C. M. Folkman, S. H. Baek, N. Balke, C. M. Brooks, D. A. Tenne, D. G. Schlom, L. Q. Chen, X. Q. Pan, S. V. Kalinin, V. Gopalan, and C. B. Eom, Phys. Rev. Lett. **104**, 197601 (2010).
[40] J. M. Garćia-Lastra, P. Garćia-Fernández, F. Calle-Vallejo, A. Trueba, J. A. Aramburu, and M. Moreno, Inorg. Chem. **53**, 6534 (2014).
[41] J. A. Aramburu, P. Garcia-Fernandez, and M. Moreno, Chem. Phys. **460**, 83 (2015).
[42] J. B. Goodenough, Phys. Rev. **100**, 564 (1955).
[43] J. Kanamori, J. Phys. Chem. Solids **10**, 87 (1959).
[44] T. Tsuyama, T. Matsuda, S. Chakraverty, J. Okamoto, E. Ikenaga, A. Tanaka, T. Mizokawa, H. Y. Hwang, Y. Tokura, and H. Wadati, Phys. Rev. B **91**, 115101 (2015).
[45] J. M. Rondinelli and N. A. Spaldin, Phys. Rev. B **81**, 085109 (2010).
[46] Y. Murakami, J. P. Hill, D. Gibbs, M. Blume, I. Koyama, M. Tanaka, H. Kawata, T. Arima, Y. Tokura, K. Hirota, and Y. Endoh, Phys. Rev. Lett. **81**, 582 (1998).
[47] P. E. Blöchl, Phys. Rev. B **50**, 17953 (1994).
[48] G. Kresse and J. Hafner, Phys. Rev. B **47**, 558 (1993).
[49] G. Kresse and J. Furthmüller, Phys. Rev. B **54**, 11169 (1996).
[50] J. P. Perdew, K. Burke, and M. Ernzerhof, Phys. Rev. Lett. **77**, 3865 (1996).
[51] A. I. Liechtenstein, V. I. Anisimov, and J. Zaanen, Phys. Rev. B **52**, R5467 (1995).
[52] J. Heyd, G. E. Scuseria, and M. Ernzerhof, J. Chem. Phys. **118**, 8207 (2003).
[53] J. Heyd, G. E. Scuseria, and M. Ernzerhof, J. Chem. Phys. **124**, 219906 (2006).
[54] E. Bousquet, M. Dawber, N. Stucki, C. Lichtensteiger, P. Hermet, S. Gariglio, J.-M. Triscone, and P. Ghosez, Nature (London) **452**, 732 (2008).
[55] See Supplemental Material at http://link.aps.org/supplemental/10.1103/PhysRevB.94.064409 for deduction of the crystal structures of $(BaMnO_3)_1/(BaFeO_3)_1$ superlattice, convergence check, and computational details of HSE06 method.
[56] R. D. King-Smith and D. Vanderbilt, Phys. Rev. B **47**, 1651 (1993).